Earthq Eng & Eng Vib (2021) 20: 803-821 **DOI**: https://doi.org/10.1007/s11803-021-2053-4

Lateral load performance and seismic demand of unbonded scrap tire rubber pad base isolators

M. B. Zisan[1†] and A. Igarashi[2‡]

1. *Department of Urban Management, Kyoto University, Kyoto 615-8540, Japan*

2. *Disaster Prevention Research Institute, Kyoto University, Kyoto 611-0011, Japan*

Abstract: The scrap tire rubber pad (STRP) made by natural or synthetic rubber and high strength reinforcing cords exhibits substantial vertical stiffness and horizontal flexibility, and these properties can be regarded as suitable for seismic isolators for structures. The use of environmentally burdensome scrap tires as STRP isolators might be convenient as an efficient and low-cost solution for the implementation of aseismic design philosophy for low-to-medium rise buildings, especially in developing countries. Finite element analyses of unbonded square and strip-shaped STRP isolators subjected to a combination of axial and lateral loads are conducted to investigate its lateral deformation performance under seismic loading. The rubber of the isolator is modelled with Mooney-Rivlin hyperelastic and Prony viscoelastic materials, including the Mullins material damage effect. The influence of the length-to-width ratio and bearing height on the isolator performance is assessed in terms of the force-displacement relationship, horizontal stiffness, damping, and isolation periods. It is shown that the dependence of stiffness on the length-to-width ratio is significant in the longitudinal direction and minor in the transverse direction. The STRP isolators following the proposed design criteria are shown to satisfy the performance requirement at different levels of seismic demand specified by the ASCE/SEI 7-2010 seismic provisions.

Keywords: lateral load; STRP isolator; length-to-width ratio; height; unbonded application; performance-based design; FEM

1 Introduction

In order to implement seismic isolation techniques in structures, several types of seismic isolators are used in structural design and construction practice. Although the steel-reinforced elastomeric isolator (SREI) is the most popular, the disadvantage of SREI is the production cost, due to labor-intensive manufacturing and vulcanization processes, making its application limited to large, expensive, and sophisticated structures as mentioned by Kelly (2002), Pan *et al*. (2005) and May (2002). May (2002) also mentioned that 'overly burdensome requirements' for design certification is a barrier to the adaption of the SREI system. To extend the earthquake-resistant design strategy for masonry structures, public buildings that include schools, hospitals, residential structures, etc., the cost reduction and simplification of the design principles are of great concern. As an alternative, several aseismic tools made of locally available inexpensive materials or lightweight materials have been proposed and investigated through experiment or finite element study by Kelly and Takhirov (2001), De la Llera *et al*. (2004), Turer and Özden (2007), Xiao *et al*. (2004), Tsang *et al*. (2012), Bandyopadhyay *et al.* (2015), Karayel *et al.* (2017) and Pistolas *et al.* (2020). The fiber-reinforced elastomeric isolator (FREI), which uses fiber reinforcement instead of steel shims, is a lightweight device and considered to offer a cost-effective design solution as proposed by Kelly (1999). The experimental and theoretical studies performed by Kelly (1997, 1999, 2002, and 2003) show that replacing steel shims in SREI with flexible fiber reinforcement yields equivalent seismic performance. An analytical solution for vertical and horizontal stiffness of FREI reinforced with flexible fiber-reinforcement is developed by Kelly and Takhirov (2001). Toopchi-Nezhad (2008a, 2008b, 2009a, 2009b, 2011, and 2014) made significant developments on FREIs through experimental and numerical studies. These studies focused on lateral load performance and the systematic design of unbonded FREIs. The findings of these studies show unbonded FREI exhibits superior performance and substantial damping. Toopchi-Nezhad *et al*. (2011), Al-Anany and Tait (2015) mentioned that the stress-strain demand in unbonded FREI is significantly lower than the bonded bearing due to the flexible fiber. Other advantages of FREI are that the device does not require any mechanical fastening and

Correspondence to: M. B. Zisan, Department of Urban Management, Kyoto University, Kyoto 615-8540, Japan
Tel: +81-70-7526-4852; Fax: +81-774-38-4147
E-mail: zisan.basir.33m@st.kyoto-u.ac.jp
[†]PhD Candidate; [‡]Professor

Received July 27, 2020; **Accepted** February 18, 2021

large endplates as those of SREI to achieve an excellent vertical and lateral performance, and consequently the production cost is reduced as mentioned by Al-Ananly *et al*. (2017).

Automobile tires are made by vulcanization of natural or synthetic rubber material with embedded reinforcing steel cords. Mishra (2012) proposed an isolator made with automobile tires called scrap tires rubber pad (STRP) isolators. The installation and operation procedures of STRP and FREI are the same. The basic difference between FREI and STRP isolator is the form of the reinforcement layer. In the STRP isolator, the steel cords are placed in the form of layers that have unidirectional resistance against elastomer bulging. On the contrary, reinforcement in FREI has bidirectional resistance against elastomer bulging. Some researchers have focused on this particular feature of tire material and explored the possibility of the application of scrap automobile tire material for seismic isolation of structures, and scrap tires are regarded as economical and environmentally friendly for the isolation of low to medium-rise buildings by Turer and Özden (2007), Spizzuoco *et al.* (2014), and Calabrese *et al.* (2015). Turer and Özden investigated the vertical and cyclic performance of unbonded stacks of tire pads through experimental study. Spizzuoco and Calabrese developed a recycled rubber-fiber reinforced bearing using a tire granule binder mixture and demonstrated that it was more advantageous than the SREI or FREI in terms of energy dissipation, manufacturing cost, and had a lighter weight. A geotechnical isolation called the RSM system is proposed by Tsang *et al.* (2012), Bandyopadhyay *et al.* (2015), and Pistolas *et al.* (2020) and composed of shredded tires and sand and was found to be very effective in reducing the effect of ground motion. An experimental study performed by Mishra (2012, 2013a and 2013b) found that the STRP has an equivalent damping ratio of approximately 10%–22% and a vertical to horizontal stiffness ratio in the range of 450–600 exceeding 150, the code specified limits. Those properties of STRP satisfy the requirement of a suitable isolation material mentioned in Kelly (1997) and Eurocode 8 (2004). Since the twisted reinforcing cords in STRP provide low flexural rigidity, Mishra and Igarashi (2013b) demonstrated that STRP exhibits a unique rollover deformation such that the bearing surfaces that initially remain in contact with supports are separated from the support faces under lateral load. Such deformation causes a reduction of horizontal stiffness followed by an accretion found by Toopachi-Nezhad *et al*. (2008a) and Osgooei *et al*. (2014). For structures made of masonry or concrete walls, Kelly (1997, 2002) and Tsai and Kelly (2002) suggest that the strip-shaped isolator is expected to be a cost-effective component of seismic isolation application since a strong base foundation layer is not required as opposed to the application of SREI. Although a strip-shaped isolator is more suitable for these types of structures, the previous studies on STRP isolators are limited to the types of slender shapes with an aspect ratio of 2.08, Van Engelen *et al*. (2015) mentioned that a low aspect ratio causes instability even at low levels of lateral strain.

The previous studies on STRP bearings highlighted the experimental evaluation of mechanical properties and force-displacement relation of STRP bearings, and loading directionality effect (Igarashi *et al*., 2013). In addition, the seismic response of a hypothetical building isolated with STRP bearings has been investigated through a pseudo-dynamic test. First, these studies considered only square-shaped isolators of low aspect ratio, which is not permitted by the design code. Second, the seismic demand of the STRP isolator determined by existing guidelines is still unknown. In the present study, both square and strip-shaped STRP isolators that satisfy the geometric criteria for stability as defined by the ASSHTO-LRFD design guidelines are investigated by 3D finite element analysis. The objectives of the study are to assess the lateral performance and seismic demand of the bearing along two orthogonal directions and the performance for different heights of STRP. A unidirectional cyclic lateral load is considered, and the strip-shaped isolators are analyzed for horizontal displacement in the longitudinal and transverse directions. The FE model is verified by comparison with the past quasi-static loading test results and a modified analytical solution. The lateral load performance of STRP isolators is evaluated in terms of load-displacement characteristics, lateral stiffness, and the effective damping ratio. The maximum bearing displacement of the STRP isolators induced by the design earthquakes is assessed using the method prescribed in the AASHTO-LRFD design guidelines to verify the feasibility of the application of the STRP isolator.

2 Scrap tire rubber pad (STRP) isolator

The preparation procedure of a STRP layer from a typical radial tire is shown in Fig. 1 by Mishra (2012). A STRP of 12 mm thickness made from Bridgestone 385/65R22.5 tires has five reinforcement layers oriented by ±70° to carcass steel, as shown in Fig. 2. A STRP isolator is made by stacking individual STRP layers one above another and then bonded by an adhesive. Table 1 shows the geometric properties of square and strip-shaped STRP isolators considered for the present study. In the case of the strip-shaped isolator, each bearing consists of two layers of STRP, which has a total height of 24 mm and a width of 72 mm. The length is varied so that the length-to-width ratio is changed between 1 and 10. The shape factor of the bearings is changed between 7.5 and 13.6. The dimensions of the strip-shaped bearings are maintained so that the aspect ratio in the length direction is equal to the aspect ratio in the width direction multiplied with the length-to-width ratio. The aspect ratio in the longitudinal direction is

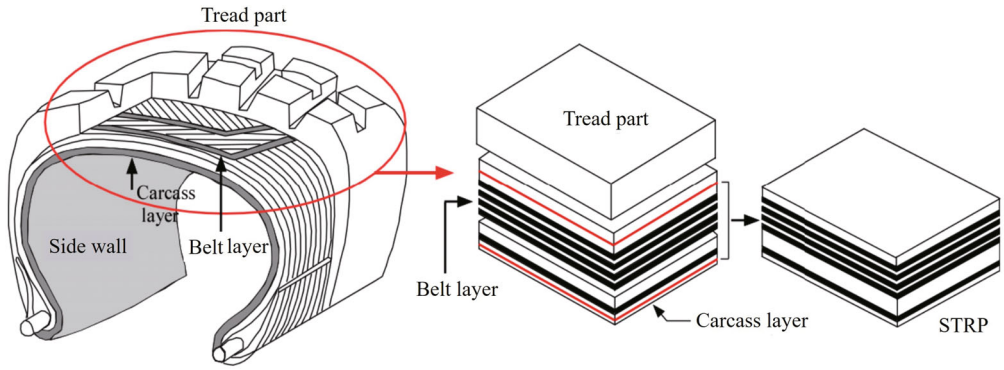

Fig. 1 Preparation of STRP specimen from scrap tires (Mishra, 2012)

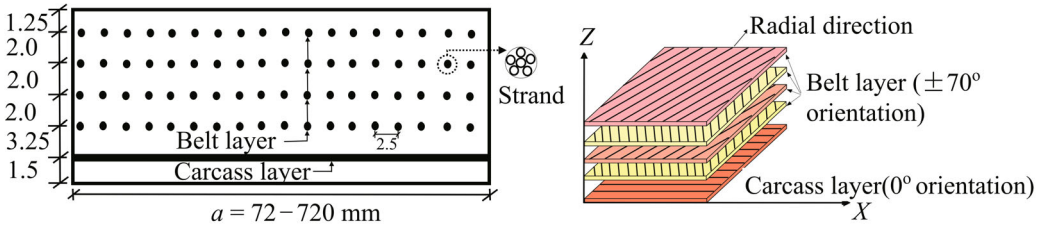

(a) 12-mm single layer STRP (b) Orientation and number of reinforcing layers (Mishra, 2012)

Fig. 2 Reinforcing steel cords in single layer STRP (Bridgestone tire 385/65*R*22.5)

Table 1 Geometric properties of STRP isolator models

Group	Designation	Dimensions $l \times w \times h$ (mm × mm × mm)	l/w	Rubber thickness t_r (mm)	Equivalent thickness t_e (mm)	Shape factor S	Aspect ratio R_x	Aspect ratio R_y
Experiment	STRP-4/1	100 × 100 × 48	1	40	2.4	10.4	2.1	2.1
Group-I: Strip-shaped	STRP-2/1	72 × 72 × 24	1	20	2.4	7.5	3	3
	STRP-2/2	144 × 72 × 24	2	20	2.4	10	6	3
	STRP-2/4	288 × 72 × 24	4	20	2.4	12	12	3
	STRP-2/10	720 × 72 × 24	10	20	2.4	13.6	3	3
Group-II: Square-shaped	STRP-1/1	36 × 36 × 12	1	10	2.4	3.75	3	3
	STRP-2/1	72 × 72 × 24	1	20	2.4	7.5	3	3
	STRP-3/1	108 × 108 × 36	1	30	2.4	11.3	3	3
	STRP-4/1	144 × 144 × 48	1	40	2.4	15	3	3
	STRP-5/1	180 × 180 × 60	1	50	2.4	18.8	3	3
	STRP-6/1	216 × 216 × 72	1	60	2.4	22.5	3	3

changed from 3.0 to 30. As for square-shaped bearings, the aspect ratio is 3.0. The thickness and the shape factor of the square-shaped isolators are varied from 12 mm to 72 mm and from 3.75 to 22.5, respectively. The equivalent thickness of the elastomer layers and that of the reinforcement layers are assumed to be 2.4 mm and 0.4 mm, respectively. An aspect ratio exceeding 2.50 mentioned by Toopchi-Nezhad *et al.* (2008b, 2009a) and Van Engelen *et al.* (2015) is assumed to meet the stability criteria. Table 1 shows the notation in the form of 'STRP-X/Y' is used to designate the type of STRP isolator model, indicating the number of the layers by X and the length-to-width ratio by Y. The isolator used in the loading test is denoted by STRP-4/1, and the test results are used for material modeling and model verification.

3 Analytical evaluation of unbonded STRP isolator

The horizontal stiffness of a bonded type bearing is given by Kelly (1997) using the following equation:

$$K_b = \frac{GA}{t_r} \tag{1}$$

in which G is the shear modulus and A is the plan area of the isolator. Ashkezari *et al*. (2008), Strauss *et al.* (2014), and Das *et al*. (2014) mentioned that the shear modulus decreases as the lateral strain increases. Strauss *et al.* (2014) demonstrated that a substantial reduction of the shear modulus takes place within the intermediate strain levels, and the shear modulus is dependent not only on the actual shear deformation but also on the maximum shear deformation ever applied to the materials. To express such strain dependence of the shear modulus, the effective modulus, proposed by Gerhaher *et al*. (2011) and Ngo *et al*. (2017) is given by

$$G_{\text{eff}}^{\text{ub}}=\begin{cases} G\left(1-\left[\dfrac{p}{p_{\text{crit},0}\left\{1-\left(\dfrac{u}{a}\right)^2\right\}}\right]^2\right)\left(1-\dfrac{u}{a}\right) & \text{for } 0\le u<t_{\text{r}} \\ G\left(1-\left[\dfrac{p}{p_{\text{crit},0}\left\{1-\left(\dfrac{t_{\text{r}}}{a}\right)^2\right\}}\right]^2\right)\left(1-\dfrac{t_r}{a}\right) & \text{for } t_{\text{r}}\le u<1.5t_{\text{r}} \end{cases} \tag{2}$$

where p is the vertical pressure on the isolator, u is the lateral displacement, a is the isolator dimension parallel to the lateral load, and t_{r} is the total rubber thickness. $P_{\text{crit},0}$ is called critical load capacity of the bearing at zero lateral strain and is given by the following expressions:

$$p_{\text{crit},0}=\frac{p_{\text{crit}}}{a^2},\quad p_{\text{crit}}=\frac{\sqrt{2}\pi GASr}{t_{\text{r}}},\quad r=\frac{a}{2\sqrt{3}} \tag{3}$$

where r is the radius of gyration and S is the shape factor defined by Kelly (2003). Although the shear modulus is assumed to be constant for a nominal shear strain of rubber (shear strain, hereafter) between 100% and 150% in the previous studies by Gerhaher and Ngo, the shear modulus has been shown to reduce, and a nonlinear reduction was observed by Mishra *et al*. (2014), Strauss *et al*. (2014) and Tsai and Hsueh (2001). Strauss *et al*. (2014) and Russo *et al*. (2013) demonstrated that shear modulus increases for shear strain exceeding 150%. In the case of unbonded applications, both friction force and friction area change as the lateral deformation increases, as shown in Fig. 3. These effects are expressed using the following expression given by Toopchi-Nezhad (2015):

$$A_{\text{eff}}=b(a-d)\quad \text{where } d=\frac{25}{16}\gamma h \tag{4}$$

in which A_{eff} is the effective bearing area that remains in contact with supports, d is the projected length of the rollover region, h is the height of the isolator, and γ is a geometric parameter defined by

$$u=\frac{25}{64}h\left[2\gamma\sqrt{1+4\gamma^2}+\ln\left(2\gamma+\sqrt{1+4\gamma^2}\right)\right] \tag{5}$$

Russo *et al.* (2013) and Pauletta *et al*. (2015) demonstrated that the horizontal displacement of a bearing required to initiate the separation of the bearing from the support faces is affected by the magnitude of axial compression. Toopchi-Nezhad ignored the effect of axial compression in their study. Moreover, the deformed shape of the stress-free side rubber surfaces tends to change from a parabolic one to a flat plane normal to the layer when the bearing displacement exceeds the rollover displacement, resulting in a reduction of shear strain and apparent stiffening of the bearing. In the current study, both rollover deformation and the effect of axial load are considered through a modified effective area, A_{effm} given by

$$A_{\text{effm}}=b\left[a-\left(d-d_0\right)\right]\quad \text{where } d_0=H\sqrt{1-\left(1-\frac{p}{E_{\text{c}}}\right)^2} \tag{6}$$

and d calculated by Eq. (4) is replaced with d–(u–1.67t_{r}) for a displacement such that $u \ge 1.67t_{\text{r}}$ to calculate the modified effective area, A_{effm}. The stiffness, K_{h} and effective damping ratio, β are evaluated by the following expressions (ASCE/SEI 7-10, 2010):

$$K_{\text{h}}=\frac{\left|F^+\right|-\left|F^-\right|}{\left|u^+\right|-\left|u^-\right|}\ \text{and}\ \beta=\frac{2}{\pi}\left[\frac{E_{\text{loop}}}{K_{\text{h}}\left(\left|u^+\right|+\left|u^-\right|\right)^2}\right] \tag{7}$$

where F^+ and F^- are the positive and negative maximum forces, u^+ and u^- are the positive and negative maximum displacements, respectively, and E_{loop} is the area of the force-displacement curve for a single loading cycle.

4 Finite element modelling

4.1 Material modelling

Table 2 shows the properties of reinforcing steel cords of the scrap tires obtained from Bridgestone 385/65*R*22.5 by Mishra *et al*. (2013a). The reinforcing cords are formed by twisted filaments with a yield strength of around 2800 MPa. The properties of tire rubber have been investigated extensively using the hyperelastic Mooney-Rivlin material model by Baranowski *et al.* (2012), Kim *et al*. (2012), and Meschke *et al*. (1997) in their studies. In the present study, the hyperelastic behavior of the rubber material is derived from the three-term Mooney-Rivlin energy function as given by

$$W=C_{10}(I_1-3)+C_{01}(I_2-3)+C_{11}(I_1-3)(I_2-3) \tag{8}$$

where C_{10}, C_{01}, and C_{11} are the material constants, and I_1 and I_2 are the first and second invariants of the Green deformation tensor. The hyperelastic material constants for Bridgestone 385/65*R*22.5 estimated by Mishra *et al*. (2013a) through uniaxial tests are shown in Table 3. The procedure to determine these material constants from a uniaxial test up to 350% axial strain can be found in Mishra *et al*. (2013a). Das *et al.* (2014) modelled the viscoelasticity of rubber using the Prony series viscoelastic shear response parameters, and the same constitutive model is considered to express the hysteretic stress-strain relationship observed in the test. The viscoelastic parameters are derived using the large strain viscoelasticity model proposed by Simo (1987) and expressed by the following equations:

$$W(E_{ij}, t) = W(E_{ij})R(t) \tag{9}$$

$$R(t)=1-\sum_{n=1}^{N}\delta^n(1-\exp(-t/\lambda^n)) \tag{10}$$

where $W(E_{ij})$ is the standard Mooney-Rivlin strain energy function given in Eq. (8) and $R(t)$ is the relaxation function in the Prony series form, δ^n is a time-dependent scalar multiplier and λ^n the is relaxation time. The elastomer softening is included using the discontinuous phenomenological damage model representing the so-called Mullins effect by

Unloading case:

$$W\frac{\partial\eta}{\partial W}+\eta=1-\frac{1}{r_1}\tanh\left[\frac{1}{m_1}\left(1-\frac{W}{W_{\mathrm{m}}}\right)\right] \tag{11}$$

Reloading case:

$$W\frac{\partial\eta}{\partial W}+\eta=1-\frac{1}{r_2}\tanh\left[\frac{1}{m_2}\left(1-\frac{W}{W_{\mathrm{m}}}\right)\right] \tag{12}$$

where r and m indicate the damage parameters and W is the Mooney-Rivlin strain energy function given in Eq. (8). An iterative procedure is employed to determine the viscoelastic parameters (δ^n, λ^n) and Mullins damage parameters (η, m) using the Eqs. (9)–(12) and the hyperelastic parameter found from the test. During each iteration, a pair of multiplier and relaxation time parameters are assumed, and then FE analysis is carried out until the hysteresis loop from the experiment is matched with the FE analysis result. The first iteration is carried out using the Prony series viscoelastic shear response parameters mentioned by Das *et al*. (2014) and damage parameters found from Feng and Hallquist (2014). The viscoelastic and Mullins damage parameters which reproduce a hysteresis curve comparable to the experiment result are listed in Table 3. These parameters are derived under the boundary conditions used in the tests. A change in the loading rate or vertical compression and the nature of the input displacement path are not considered for material parameters.

4.2 Modelling of STRP isolator

FE analysis of the STRP isolator models described in the previous section is carried out by MSC Marc-Mentat (2018). An isoperimetric hexahedron element of Herrmann type is used for the rubber material. The reinforcing steel cords in the rubber composite are represented by a hollow and isoperimetric rebar element. Figures 4(a) and 4(b) show the FE model of STRP-4/1 and STRP-2/4 isolators, respectively. The

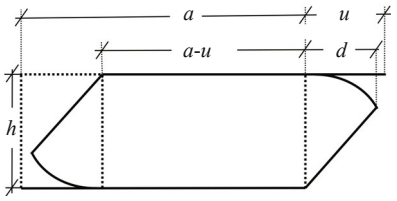

Fig. 3 Lateral deformation of unbonded STRP isolator

Table 2 Properties of reinforcing cord

Layer	Layer No.	No. of Filaments	Filament dia (mm)	Single cord area (mm^2)	Orientation	Equivalent thickness t_f (mm)	Yield Strength (MPa)	Spacing (mm)	E (GPa)	v
Carcass	1	5	0.2	0.44	0°	0.40	2800	2.5	200	0.3
Belt	4	14	0.4	0.63	∓ 70°	0.40	2800	2.5	200	0.3

Table 3 Properties of elastomer

Mooney-Rivlin constant			Shear modulus (MPa)			Prony shear responses				Mullin-damage parameters			
C_{10}	C_{01}	C_{11}	G_{eff}	G	v	δ^1	λ^1	δ^2	λ^2	η_1	m_1	η_2	m_2
0.40	1.22315	0.18759	1.10	1.31	0.49995	0.30	0.2	0.30	0.55	0.01	5	0.05	10

bottom and top contact surfaces are modelled as a rigid plane, as shown in Fig. 4. All degrees of freedom of the bottom surface and rotational degrees of freedom of the top surface are constrained. Axial force and lateral displacement are applied at the top surface. Figure 4(c) shows the pattern of external lateral displacement used in the experiment and FE analysis. The contact between the adjacent layers of STRP is assumed as a glue contact so that any detachment or slip between the layers is not allowed. The friction coefficient recommended for tire-dry asphalt is 0.7, that for tire-concrete is 1.0, and that for rubber-rubber is 1.15, as described by Glenn (2006). The contact surface between the rubber layer and the rigid surface is specified as touch contact using the bilinear Coulomb friction model with a friction coefficient of 0.80. In touch contact, each rubber node is constrained along the direction normal to the contact surface and detaching of the rubber node from the contact surface is allowed. In order to accurately simulate the contact and friction behavior, the segment-to-segment contact algorithm is used. The so-called mixed-method based on Herrmann′s formulation recommended in large-strain analysis for elastomer rubber is used. The geometric nonlinearities are incorporated using the updated Lagrangian formulation.

5 FE model verification

In order to check the validity of the application of the modified method to STRP isolators, lateral stiffness estimated by the modified method is compared with the stiffness obtained in experimental studies by Toopchi-Nezhad (2008a), Al-Anany (2017), and Mishra (2013a). A comparison of lateral stiffness is shown in Fig. 5, in which the notations “EX”, “EM” and “MM” indicate the experiment, the existing method, and the modified method, respectively. Similarly, “ISO” and “NRB” stand for isolator and natural rubber bearing, respectively. In the low shear strain range of less than 150%, stiffness found from the existing solution is comparable with the experimental result, and the modified solution provides a slightly higher value than the existing method because of the compression effect. However, for a

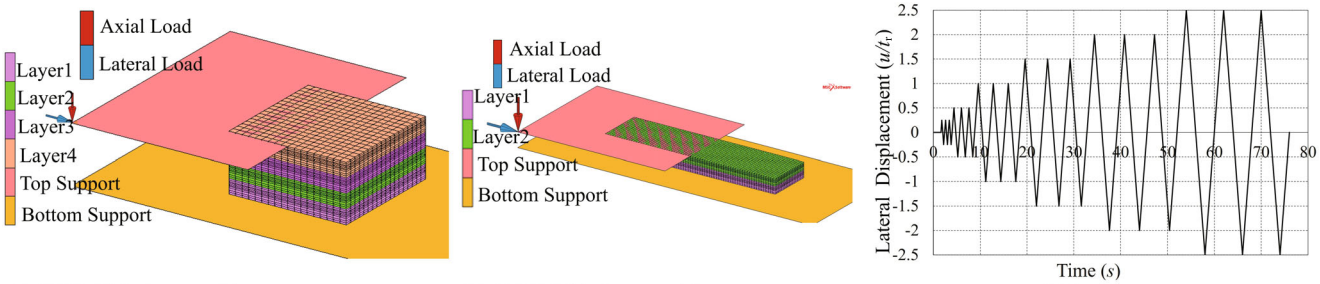

(a) STRP-4/1 isolator model (b) STRP-2/4 isolator model (c) Loading pattern

Fig. 4 FE model and boundary conditions, and lateral loading condition

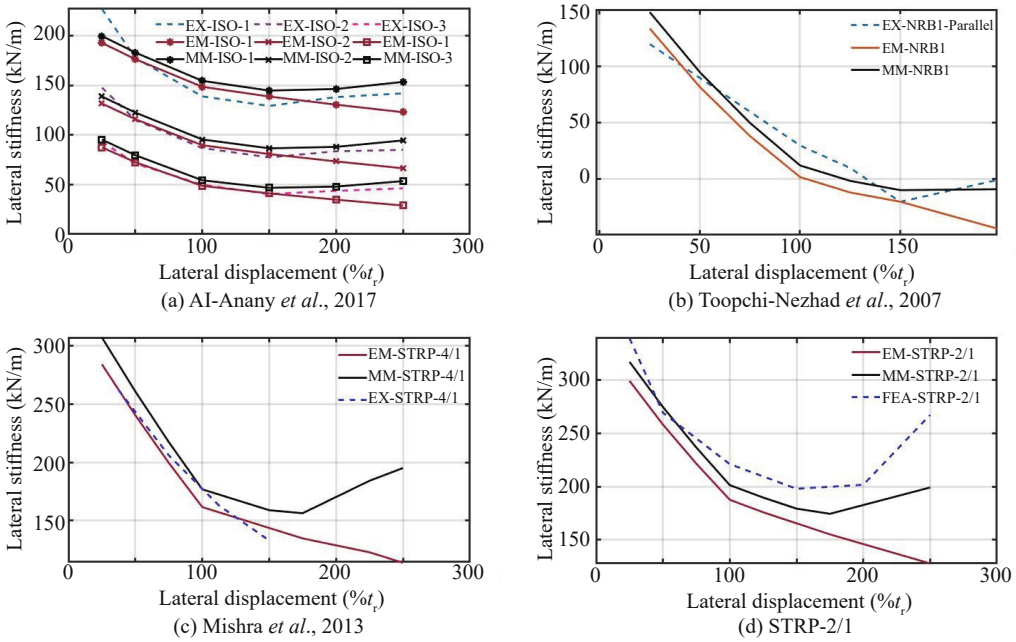

(a) AI-Anany *et al*., 2017 (b) Toopchi-Nezhad *et al*., 2007

(c) Mishra *et al*., 2013 (d) STRP-2/1

Fig. 5 Comparison of lateral stiffness vs. displacement relationship

displacement exceeding 150%, the existing method significantly underestimates the stiffness obtained by the experimental results. The reason is that the bearing's rollover deformation is ignored in the existing method proposed by Toopchi-Nezhad (2014) and Konstantinidis and Kelly (2014) when deformation exceeds the limit shear strain of 167% at which the vertical rubber surfaces of the isolator touch the support faces. Figures 5(a) and 5(b) show that the modified method provides a considerably close prediction of the experimental result at all displacement ranges.

Based on the analytical result using the modified method, the correctness of the FE models is discussed. Compared with the result of Mishra *et al*. (2013a) shown in Fig. 5(c) and the FE analysis result of STRP-2/1 shown in Fig. 5(d), the estimated value by the modified method is smaller and deviates from the FE analysis at a large displacement. Table 4 shows the comparison of stiffness values of STRP-4/1 at four displacements, obtained by the past cyclic loading test, FE analysis, and the modified method. Good agreement can be seen among these stiffness values. The hysteresis curve obtained from the FE analysis in comparison with the test result is shown in Fig. 6(a). It is shown that the accuracy of the FE model is acceptable. In particular, the average value of the effective stiffness for STRP-4/1, defined by the slope of the hysteresis curve in Fig. 6(a) (dashed line) and estimated by least square curve fitting, is found to be about 124.5 kN/m by Mishra and Igarashi (2013b) and the FE analysis. The FE analysis gives effective damping of around 14%–16%, and its average is 16.9% higher than the average of the experiment results. The premise is that the damping in the STRP isolator appears when rubber is combined with the embedded steel cords, possibly due to the friction within the steel cord consisting of multiple steel strands. In the FE analysis, the damping property of the STRP is modelled by hysteretic energy dissipation in the rubber as a compromised approximation for the convenience of numerical computation.

In a similar manner, the hysteretic behavior of STRP-2/1 is estimated using the FE analysis. The hysteresis loop of STRP-2/1 is shown in Fig. 6(b). The stiffness obtained from the FE analysis and that by the proposed evaluation are included in Table 4, which indicates that both results show a good agreement. Moreover, the effective damping of STRP-2/1 computed by the FE analysis reasonably conforms to that of the STRP-4/1 at all displacement amplitudes. Therefore, the FE model of STRPs can be regarded as consistent and congruous with the test result and analytical solution.

6 Lateral performance of STRP isolator

6.1 Load-displacement relationships

Figures 7 and 8 show the normalized force-displacement curves of the STRP-2/1, 2/2, 2/4, and 2/10 strip-shaped isolators, for longitudinal and transverse loading, respectively. The hysteretic performance of each bearing is evaluated under 5.0 MPa vertical pressure, which is the average of lower and upper limits of mean vertical pressure defined by CAN/CAS-S6 (2006) and AASHTO-LRFD specifications (2014). Also, each bearing is subjected to a horizontal displacement up to 250% shear strain. These hysteresis curves indicate that each isolator under the specified compression level exhibits a stable rollover behavior and displays no slippage within the lateral displacement corresponding to 250% shear strain. Therefore, the minimum aspect ratio of 3.0 recommended in the AASHTO-LRFD method A for bonded type isolators can also be used for the unbonded case as a stability requirement at 5.0 MPa compression. According to Figs. 7 and 8, a large value of the length-to-width ratio induces the onset of hardening at a lower strain level and subsequent rapid increase of the restoring force. For example, the hardening in STRP-2/2, 2/4, and 2/10 initiates from a displacement exceeding 100% shear strain in the longitudinal direction as shown in Figs. 7(b) to 7(d), whereas the hardening in the transverse direction starts from 150% shear strain, indicated by Fig. 8. In both directions, STRP-2/1 shows that hardening initiates from 150% shear strain. A comparison of these hysteresis curves shows that the contribution of the rollover part in the restoring force is increased for bearings with a low aspect ratio like

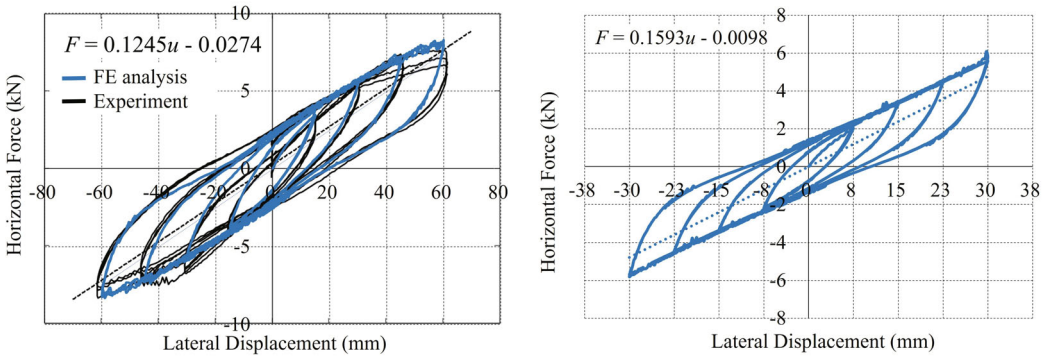

(a) Load-displacement curve of STRP-4/1 (b) Load-displacement curve of STRP-2/1

Fig. 6 Hysteresis curve obtained by FE analysis

STRP-2/1 in Fig. 7(a), while the contribution becomes negligible for aspect ratios greater than 5.0 as STRP-2/10 in Fig. 7(d).

Figure 9(a) shows the deformed shapes of the STRP-2/1 isolator at different levels of longitudinal displacements. Top and bottom surfaces of the isolator roll-off from the contact surfaces, resulting in a reduction of the shear area on the contact surface. The shear area reduction continues until the vertical side surfaces of the bearing come in contact with the surface as shown in Fig. 9(b). This result conforms with the deformed shape of the STRP isolator models observed during loading tests (Mishra and Igarashi, 2103b).

The normalized force-displacement curves of the square-shaped isolators for different numbers of stacked STRPs are shown in Fig. 10. Each bearing has an aspect ratio of 3.0 and is subjected to shear loading of up to 250% shear strain under axial compression of 5.0 MPa. These figures indicate that each bearing displays a positive increment of lateral force and no slippage up to 250% shear strain. It implies that the number of stacks does not affect the lateral stability if the aspect ratio is maintained at 3.0. Therefore, an aspect ratio of 3.0 is suitable against instability without regard for the height of an unbonded STRP isolator. The normalized value of the maximum restoring force of stacked STRPs at 250%

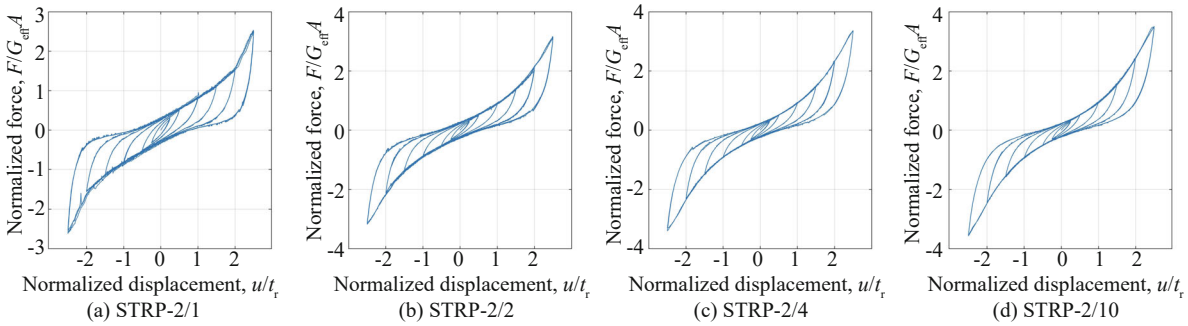

Fig. 7 Hysteresis curve for longitudinal loading under 5.0 MPa compression

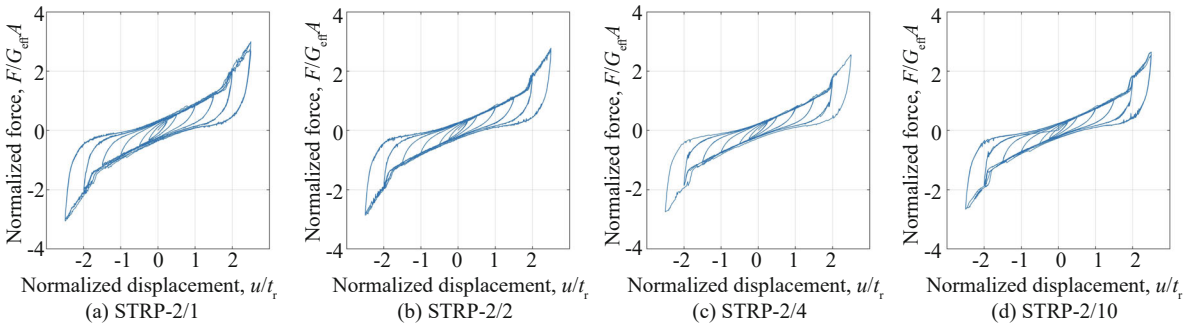

Fig. 8 Hysteresis curve for transverse loading under 5.0 MPa compression

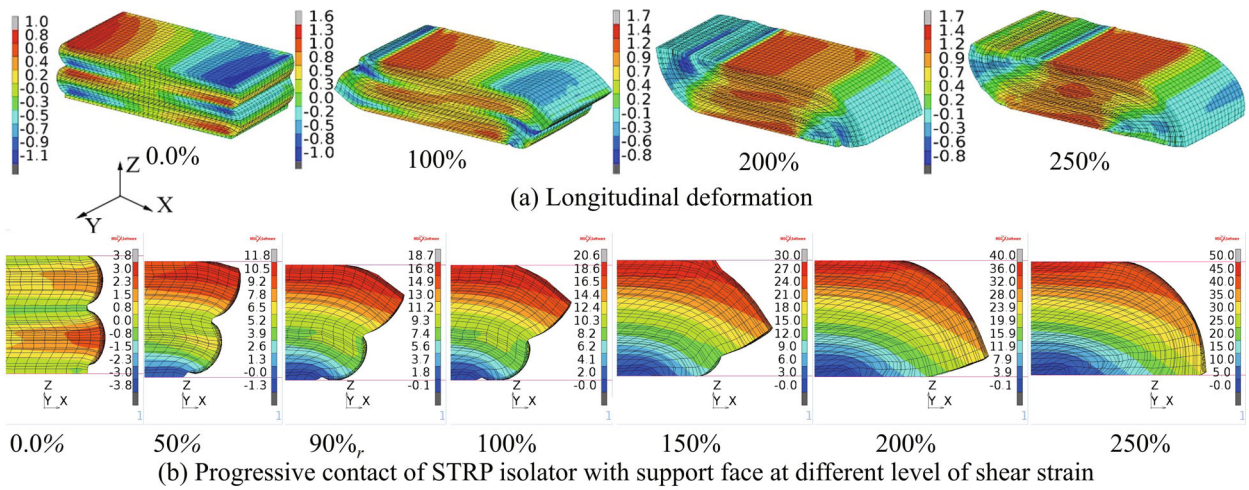

Fig. 9 Lateral deformation of unbonded STRP isolator

shear strain is almost unaffected by the number of STRP stacks. The area of the hysteresis loop for any number of STRP stacks exceeding 3.0 is nearly the same.

6.2 Horizontal stiffness and effective damping ratio

The values of stiffness and damping ratio of the strip-shaped STRP isolators obtained from FE analysis are shown in Tables 5 and 6. Figure 11 shows the plots of normalized lateral stiffness and the longitudinal-to-transverse stiffness ratio at different levels of lateral strains and length-to-width ratios. The dashed line indicates the stiffness obtained from the modified stiffness solution, while the solid line indicates that of the FE analysis result. The stiffness of square-shaped STRP-2/1 obtained by the modified method shows good agreement with the FE analysis result for displacements up to 150% shear strain. However, the FE analysis result for displacement exceeding 150% shear strain is found to be higher than the values obtained by the modified method. For the other isolators, the transverse stiffness is comparable with that from the modified method for displacements up to 100% shear strain and the modified method provides good estimates of the longitudinal stiffness only for a displacement of 25% shear strain. In summary, the modified method results in higher stiffness in the intermediate displacement range and lower stiffness in the higher displacement range. The possible reasons for this discrepancy are the following two factors: the effect of the length-to-width ratio and distinctive rollover peculiar to the STRP isolator, as shown in Fig. 9. The STRP isolator displays a progressive

Table 4 Horizontal stiffness and damping: Experimental, FEA and evaluation by modified method (MM)

Bearing	u (%t_r)	Horizontal stiffness, K_h (kN/m)					Effective damping		
		Experiment	FEA	MM	Exp/FEA	FEA/MM	Experiment	FEA	Exp/FEA
STRP-4/1	37.5	262	258	263.7	1.02	0.98	13.2	15.3	0.86
	75.0	206	190	188.0	1.08	1.01	12.2	16.5	0.74
	112.5	163	163	138.0	1.00	1.18	14.2	15.8	0.90
	150.0	133	137	120.0	0.97	1.14	15.0	16.4	0.91
STRP-2/1	37.5	---	298	294.4	---	1.01	---	15.5	---
	75.0	---	229	236.3	---	0.97	---	16.4	---
	112.5	---	201	196.3	---	1.02	---	15.2	---
	150.0	---	194	179.8	---	1.08	---	14.2	---

Table 5 Horizontal stiffness and damping of STRP-2 isolator under longitudinal loading

Normalized displacement (u/t_r)	STRP-2/1		STRP-2/2		STRP-2/4		STRP-2/10	
	K_h (kN/m)	Damping β (%)	K_h (kN/m)	Damping β (%)	K_h (kN/m)	Damping β (%)	K_h (kN/m)	Damping β (%)
$0.25t_r$	339.2	14.31	658.6	12.04	1296.4	11.76	3229.3	11.7
$0.5t_r$	269.3	16.63	528.6	14.59	1071.4	13.69	2699.3	13.5
$1.0t_r$	221.1	15.45	461.8	12.91	970.0	11.93	2500.7	11.6
$1.5t_r$	198.0	14.66	477.3	11.04	1045.4	9.95	2720.8	9.6
$2.0t_r$	201.7	13.39	549.6	9.50	1211.6	8.74	3182.5	8.4
$2.5t_r$	267.3	11.00	657.6	8.85	1404.0	8.40	3670.7	8.2

Table 6 Horizontal stiffness and damping of STRP-2 isolator under transverse loading

Normalized displacement (u/t_r)	STRP-2/1		STRP-2/2		STRP-2/4		STRP-2/10	
	K_h (kN/m)	Damping β (%)	K_h (kN/m)	Damping β (%)	K_h (kN/m)	Damping β (%)	K_h (kN/m)	Damping β (%)
$0.25t_r$	350.9	12.95	630.1	12.44	1203.0	10.97	2928.3	12.3
$0.5t_r$	274.2	16.10	493.5	15.11	949.5	14.63	2345.0	14.4
$1.0t_r$	222.1	15.09	406.1	14.13	794.5	13.48	1970.8	13.2
$1.5t_r$	205.9	13.85	386.7	12.74	759.6	12.26	1867.4	12.1
$2.0t_r$	268.0	10.66	490.4	9.89	941.5	9.76	2371.5	9.5
$2.5t_r$	314.2	10.77	586.2	9.88	1101.3	10.08	2755.8	9.8

rollover deformation leading to touching of the vertical side face on the support face at a displacement of 90% shear strain. As shown in Fig. 9(b), the area of touching keeps growing until a displacement of 250% shear strain, instead of 167% shear strain generally observed for FREI in Konstantinidis and Kelly (2014). The feature of STRP isolators regarding this progressive contact makes the device more restrained and stable, and this property becomes more visible with the increase of the length-to-width ratio.

Figure 11 shows that as the length-to-width ratio increases, the longitudinal stiffness increases, whereas the transverse stiffness shows a minor decrease. For example, comparing STRP-2/1 and STRP-2/10, longitudinal stiffness increased by 37.4%, 57.8% and 37.5% at the displacement of 150%, 200% and 250% shear strain, respectively. At the same displacement levels, these variations estimated from the modified solution are higher than those of the FE analysis results. The contribution of the rollover zone in Eq. (6) is high for an isolator with a low length-to-width ratio considers for such differences. On the other hand, the transverse stiffness decreased by 12% on average at each level of lateral displacement. Therefore, a high value of length-to-width ratio reduces the efficiency of isolation of a strip-shaped isolator in the longitudinal direction. Figure 11(c) shows the relationship of the longitudinal-to-transverse stiffness ratio and the lateral displacement. As the length-to-width ratio increases, stiffness in the longitudinal direction increases by 1.15–1.40 times.

Figure 12 shows the effective damping ratios obtained from the FE analysis results ranging between 8%–16%. This result shows that the minimum effective damping ratio of the strip-shaped STRP isolator is found to be approximately 8% for the longitudinal direction and 10% for the transverse direction. The effective damping ratio tends to be lower for a high value of length-to-width ratio. The length-to-width ratio as high as 10 causes an average damping reduction of about 26.5% and 10.3% at each level of lateral displacement in the longitudinal

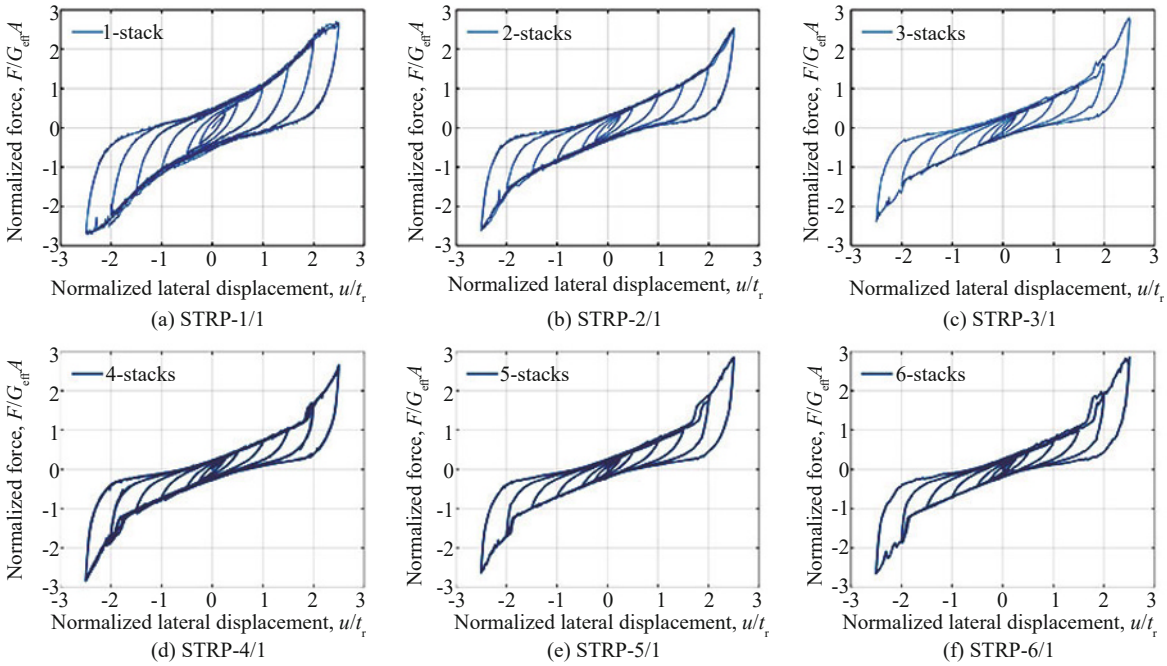

Fig. 10 Normalized force-displacement relations for different number of stacked STRPs

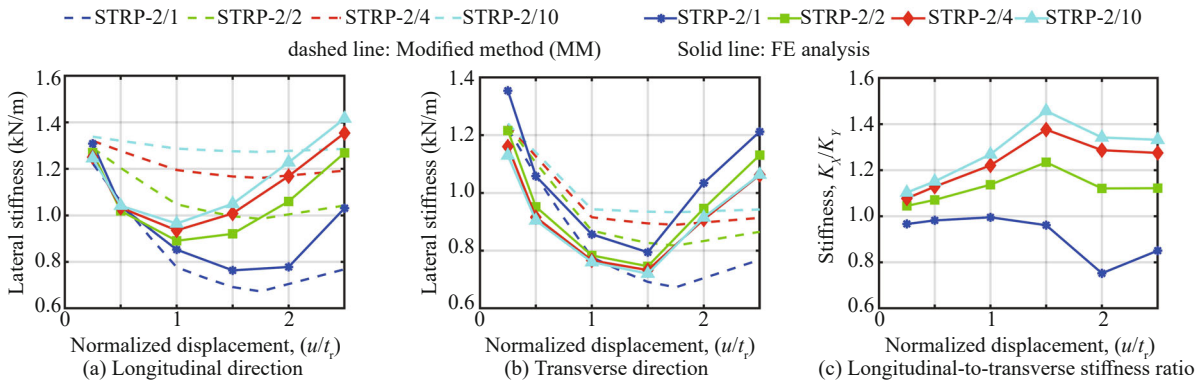

Fig. 11 Relationship between horizontal stiffness and lateral displacement

and transverse directions, respectively. For displacement at 250% shear strain, the isolators′ effective damping ratio decreased by 38% and 33% on average for the longitudinal and transverse directions, respectively, concerning 25% shear strain. The effect of hardening at large shear displacement results in an improvement of stiffness as well as a reduction of damping. The damping of the strip-shaped bearing is higher in the transverse direction than in the longitudinal direction, as given in Fig. 12(c). The specified minimum damping in the design recommendation should be selected considering these properties of the STRP isolator.

Table 7 shows the stiffness and damping values of the square-shaped bearing with a different number of stacks of STRP. The number of stacks increases from 1 to 6 and each of the stacks is 12 mm thick. The aspect ratio is assumed to be equal to 3.0 for all isolators. Each isolator is compressed by 5.0 MPa pressure first and then subjected to shear loading up to 250% shear strain in the carcass direction. Figure 13 shows the normalized stiffness and damping ratio for a different number of stacks. Although the normalized stiffness decreases as the number of stacks increases, the variation of the values are within ±10% of the average value for 2 or more stacks. Therefore, horizontal stiffness increases approximately in proportion with the number of stacks provided that the aspect ratio is maintained as 3.0. The damping ratios decrease by 10%–20% as the number of stacks increases from two to six, and the minimum damping is about 9% for the six-stacked STRP isolator. Due to a fixed aspect ratio, the shape factor increases with an increase in the stack numbers. The isolator made of a single stack or two stacks suffers comparatively high lateral bulging that influences the restoring force characteristics under lateral displacement. It is considered as a reason for different hysteresis behavior and damping when stack numbers increases.

7 Seismic demand evaluation

In this section, the seismic demand to the strip-shaped STRP isolators is assessed to check their feasibility under example building design conditions that can be encountered in application practice. The equivalent lateral force (ELF) procedure is considered for the seismic design of low-rise buildings with a regular plan. The advantage of the ELF method in the analysis of low-rise buildings is that the displacement in the first mode is mainly concentrated at the isolator. The assessment is carried out for two levels of design earthquakes: design basis earthquake (DBE) and maximum considered earthquake (MCE). The maximum design lateral displacement (D_D) and the effective period (T_D) of an STRP isolator are determined by

$$D_D = \frac{gS_{D1}T_D}{4\pi^2 B_D} \text{ and } T_D = 2\pi\sqrt{\frac{W}{K_{hmin}g}} \tag{13}$$

where g is the gravitational acceleration, T_D is the

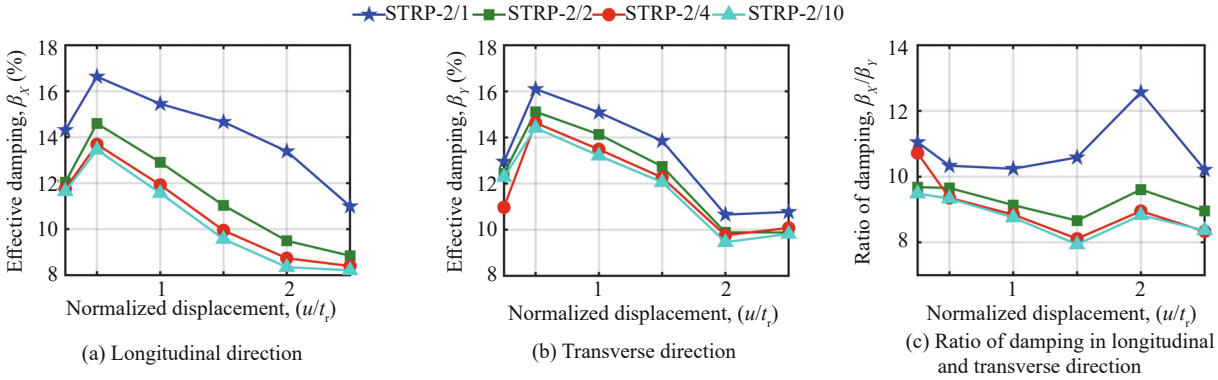

Fig. 12 Effective damping vs. lateral displacement obtained by FE analysis

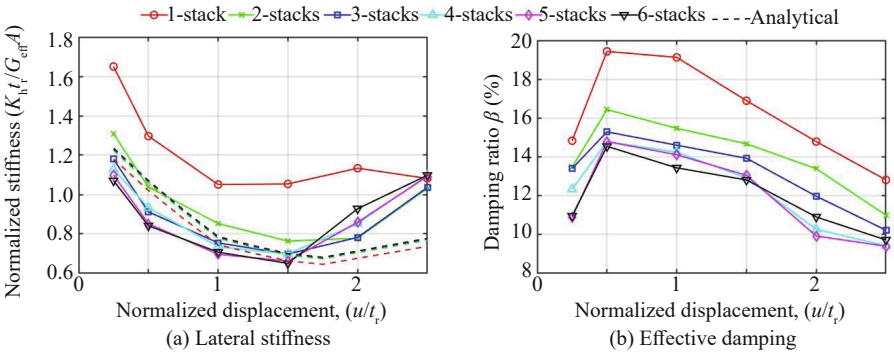

Fig. 13 Normalized stiffness and damping ratio for different number of stacked STRPs

isolation period, W is the effective seismic weight, and K_{hmin} is the minimum effective stiffness, B_D is the damping coefficient, and S_{D1} is 5% damped DBE spectral acceleration at a period of 1 s and is given by

$$S_{M1} = F_v S_1 \quad \text{and} \quad S_{D1} = 2/3\, S_{M1} \tag{14}$$

in which S_1 is risk-targeted MCE spectral acceleration for a period of 1 s, and F_v is the site class coefficient obtained from ASCE/SEI 7-10. For the MCE level, displacement, D_M and period, T_M are obtained by replacing the suffix D by M in Eq. (14). An iterative procedure described by Toopchi-Nezhad *et al*. (2008a) and shown in Fig. 14 is used to calculate the displacement and the period satisfying Eq. (13).

7.1 Performance of Strip-shaped STRP isolator

The isolation period and displacement demand at DBE and MCE spectral accelerations are estimated based on the stiffness and damping listed in Tables 5 and 6 of the 1/4th scale prototype models (Group-I). The displacement, period, and stiffness of the full-scale model are equal to four, two, and four times, respectively, of the 1/4 th scale model, following the similitude law followed by Kim *et al*. (2009). Therefore, the plan areas of the full-scale models are determined to be 288 mm × 288 mm, 576 mm × 288 mm, 1152 mm ×288 mm, and 2880 mm × 288 mm, and the height is 96 mm. Each isolator carries a seismic weight that produces a pressure equal to 5.0 MPa. It is assumed that allowable shear strains at DBE and MCE levels should be within 100%–150%

Table 7 Horizontal stiffness and damping of square-shaped STRP isolator for loading in the carcass direction

Normalized displacement (u/t_r)	STRP-1/1 1-stack		STRP-2/1 2-stacks		STRP-3/1 3-stacks		STRP-4/1 4-stacks		STRP-5/1 5-stacks		STRP-6/1 6-stacks	
	K_h (kN/m)	Damping β (%)	K_h (kN/m)	Damping β (%)	K_h (kN/m)	Damping β (%)	K_h (kN/m)	Damping β (%)	K_h (kN/m)	Damping β (%)	K_h (kN/m)	Damping β (%)
$0.25t_r$	213.9	14.8	350.9	12.95	458.6	13.4	585.1	12.3	712.4	10.9	832.5	10.96
$0.5t_r$	168.1	19.4	274.2	16.10	354.6	15.3	483.7	14.8	551.8	14.8	654.3	14.54
$1.0t_r$	136.2	19.1	222.1	15.09	293.5	14.6	381.2	14.2	451.4	14.1	550.1	13.44
$1.5t_r$	136.6	16.9	205.9	13.85	271.4	13.9	362.0	12.9	429.0	13.1	505.9	12.81
$2.0t_r$	146.9	14.8	268.0	10.66	304.2	12.0	442.1	10.3	557.0	9.9	721.8	10.91
$2.5t_r$	140.2	12.8	314.2	10.77	402.9	10.2	569.0	9.4	707.7	9.4	853.9	9.72

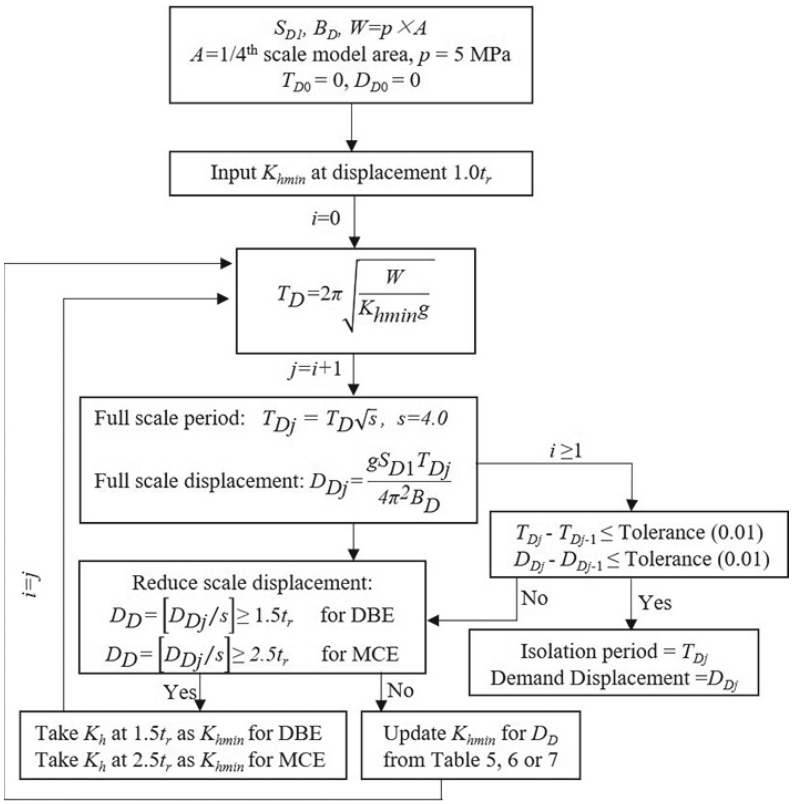

Fig. 14 Flowchart for seismic demand calculation

and 200%–250%, respectively. The minimum effective damping ratio and the corresponding damping coefficient, B_D and B_M for the DBE and MCE level displacements, chosen to be 100% and 250% shear strain, are listed in Tables 8, 9, and 10. Each iteration begins with an initial stiffness, K_{hmin} taken at 100% shear strain. The seismic performance described here is applicable only for lateral load acting along one of the principal axes of the isolator. The assessment procedure is carried out for the following three cases with different levels of seismicity:

- Case 1: Ground condition: class C site, S_1=0.40, S_{D1}=0.373 g, and S_{M1}=0.56 g
- Case 2: Ground condition: class D site, S_1=0.40, S_{D1}=0.43 g, and S_{M1}=0.64 g
- Case 3: Ground condition: class D site, S_1=0.50, S_{D1}=0.5 g, and S_{M1}=0.75 g

The assessment results for Cases 1, 2, and 3 are summarized in Tables 8, 9, and 10, respectively. The isolation periods of a 96 mm thick isolator at DBE and MCE levels ($T_D \approx 1.23$–1.48 s and $T_M \approx 1.11$–1.40 s) for each seismicity level are substantially longer than 1.0 s, and Skinner *et al*. (1993) mentioned that an earthquake contains maximum energy within the period below 1.0 s. Following the similitude law, a 200 mm thick STRP isolator can be more useful for isolation that provides an isolation period exceeding 2.0 s. Tables 8, 9, and 10 show that the maximum shear strain of the STRP isolators almost satisfies the allowable limit of 150% (DBE) and 250% (MCE) in all three cases.

Figure 15 shows the relationship between the equivalent natural period and the length-to-width ratio. It is observed that the natural period decreases by 12%–15% in the longitudinal direction (X) as the length-to-width ratio increases from unity to 10, whereas the tendency of the natural period in the transverse direction (Y) is the opposite. Figure 16 shows the relationship between the maximum shear-strain vs. the length-to-width ratio. Both at DBE and MCE levels, the transverse displacement increases as the value of the length-to-width ratio increases while the longitudinal displacement is reduced. The effect of the length-to-width ratio on the displacement conforms to the change of isolation period, as shown in Fig. 15.

Figure 17 shows the relationship between the seismic response coefficient (C_s) and the length-to-width ratio. The seismic response coefficient is defined by the ratio of total base shear to the structure′s weight. The base shear is calculated by the bearing displacement at DBE and MCE multiplied by the corresponding stiffness obtained from Tables 5 and 6. It shows that the seismic response coefficient is the same for any values of the length-to-width ratio in the transverse direction in each seismic case. On the other hand, the coefficient increases around 16% both in DBE and MCE levels as the length-to-width ratio increases from unity to 10 in the longitudinal direction. The seismic response coefficient increases with the seismicity of the site class.

8 Minimum height for effective isolation

A typical earthquake ground motion record contains a substantial amount of energy within a period range of 0.1 s–1.0 s and a maximum in the range of 0.2 s–0.6 s (Skinner *et al*., 1993). Therefore, the height of an isolator that provides a period longer than 1.0 s is defined as the

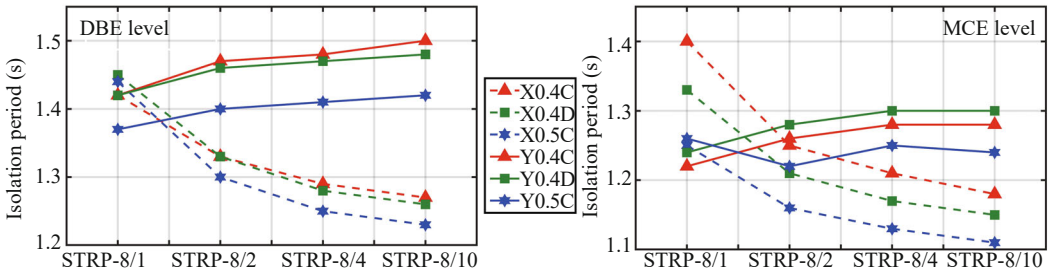

Fig. 15 Isolation period of 96 mm Strip-STRP isolator (*X*: Longitudinal, *Y*: Transverse)

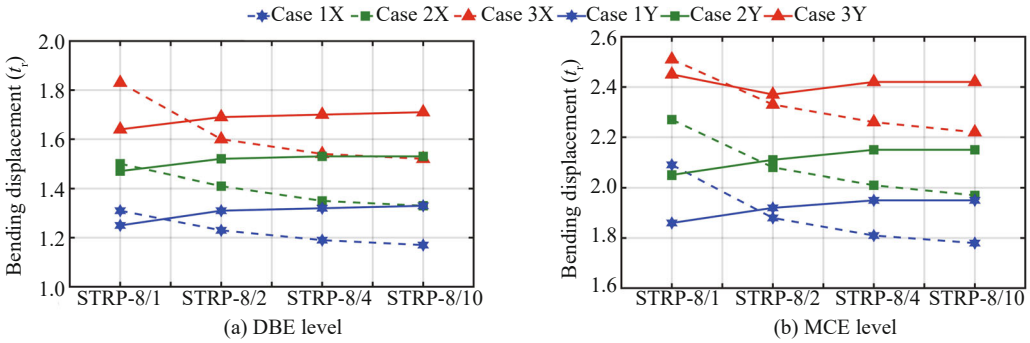

Fig. 16 Maximum displacement of 96 mm Strip-STRP isolator (*X*: Longitudinal, *Y*: Transverse)

Table 8 Performance for case-1 (Class C site, S_1= 0.40)

1/4th scale model	Full scale model dimension (mm × mm × mm)	Damping β		Damping coefficient		Spectral acceleration		Isolation periods (s)		Max. shear strain	
		DBE	MCE	B_D	B_M	S_{D1}	S_{M1}	DBE	MCE	DBE	MCE
Longitudinal direction											
STRP-2/1	STRP-8/1: 288×288×96	12%	9%	1.26	1.16	0.373 g	0.56 g	1.42	1.40	1.31	2.09
STRP-2/2	STRP-8/2: 576×288×96	12%	9%	1.26	1.16	0.373 g	0.56 g	1.33	1.25	1.23	1.88
STRP-2/4	STRP-8/4: 1152×288×96	12%	9%	1.26	1.16	0.373 g	0.56 g	1.29	1.21	1.19	1.81
STRP-2/10	STRP-8/10: 2880×288×96	12%	9%	1.26	1.16	0.373 g	0.56 g	1.27	1.18	1.17	1.78
Transverse direction											
STRP-2/1	STRP-8/1: 288×288×96	13%	10%	1.29	1.20	0.373 g	0.56 g	1.42	1.22	1.25	1.86
STRP-2/2	STRP-8/2: 576×288×96	13%	10%	1.29	1.20	0.373 g	0.56 g	1.47	1.26	1.31	1.92
STRP-2/4	STRP-8/4: 1152×288×96	13%	10%	1.29	1.20	0.373 g	0.56 g	1.48	1.28	1.32	1.95
STRP-2/10	STRP-8/10: 2880×288×96	13%	10%	1.29	1.20	0.373 g	0.56 g	1.50	1.28	1.33	1.95

Table 9 Performance for case-2 (Class D site, S_1= 0.40)

1/4th scale model	Full scale model dimension (mm × mm × mm)	Damping β		Damping coefficient		Spectral acceleration		Isolation periods (s)		Max. shear strain	
		DBE	MCE	B_D	B_M	S_{D1}	S_{M1}	DBE	MCE	DBE	MCE
Longitudinal direction											
STRP-2/1	STRP-8/1: 288×288×96	12%	9%	1.26	1.16	0.43 g	0.64 g	1.45	1.33	1.50	2.27
STRP-2/2	STRP-8/2: 576×288×96	12%	9%	1.26	1.16	0.43 g	0.64 g	1.33	1.21	1.41	2.08
STRP-2/4	STRP-8/4: 1152×288×96	12%	9%	1.26	1.16	0.43 g	0.64 g	1.28	1.17	1.35	2.01
STRP-2/10	STRP-8/10: 2880×288×96	12%	9%	1.26	1.16	0.43 g	0.64 g	1.26	1.15	1.33	1.97
Transverse direction											
STRP-2/1	STRP-8/1: 288×288×96	13%	10%	1.29	1.20	0.43 g	0.64 g	1.42	1.24	1.47	2.05
STRP-2/2	STRP-8/2: 576×288×96	13%	10%	1.29	1.20	0.43 g	0.64 g	1.46	1.28	1.52	2.11
STRP-2/4	STRP-8/4: 1152×288×96	13%	10%	1.29	1.20	0.43 g	0.64 g	1.47	1.30	1.53	2.15
STRP-2/10	STRP-8/10: 2880×288×96	13%	10%	1.29	1.20	0.43 g	0.64 g	1.48	1.30	1.53	2.15

Table 10 Performance for case-3 (Class D site, S_1= 0.50)

1/4th scale model	Full scale model dimension	Damping β		Damping coefficient		Spectral acceleration		Isolation periods (s)		Max. shear strain	
		DBE	MCE	B_D	B_M	S_{D1}	S_{M1}	DBE	MCE	DBE	MCE
Longitudinal direction											
STRP-2/1	STRP-8/1: 288×288×96	12%	9%	1.26	1.16	0.5 g	0.75 g	1.44	1.25	1.83	2.51
STRP-2/2	STRP-8/2: 576×288×96	12%	9%	1.26	1.16	0.5 g	0.75 g	1.30	1.16	1.60	2.33
STRP-2/4	STRP-8/4: 1152×288×96	12%	9%	1.26	1.16	0.5 g	0.75 g	1.25	1.13	1.54	2.26
STRP-2/10	STRP-8/10: 2880×288×96	12%	9%	1.26	1.16	0.5 g	0.75 g	1.23	1.11	1.52	2.22
Transverse direction											
STRP-2/1	STRP-8/1: 288×288×96	13%	10%	1.29	1.20	0.5 g	0.75 g	1.37	1.26	1.64	2.45
STRP-2/2	STRP-8/2: 576×288×96	13%	10%	1.29	1.20	0.5 g	0.75 g	1.40	1.22	1.69	2.37
STRP-2/4	STRP-8/4: 1152×288×96	13%	10%	1.29	1.20	0.5 g	0.75 g	1.41	1.25	1.70	2.42
STRP-2/10	STRP-8/10: 2880×288×96	13%	10%	1.29	1.20	0.5 g	0.75 g	1.42	1.24	1.71	2.42

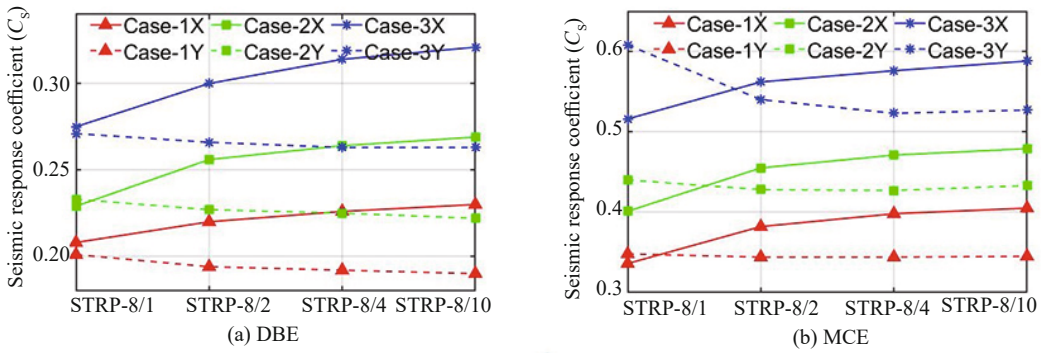

Fig. 17 Seismic response coefficient (C_s) of 96 mm Strip-STRP isolator (*X*: Longitudinal, *Y*: Transverse)

minimum height for effective isolation and preferable for seismic mitigation of a low-medium-rise building with a fixed base period in the range of 0.1 s–0.5 s. It is expected that the period elongation results in a reduction of seismic load demand to the building and of the excitation of higher modes. For a fixed magnitude of static load, the isolation period primarily depends on the lateral stiffness determined by the shear modulus, thickness, and plan dimensions of the elastomer. In this section, the relationship between the STRP isolator height and isolation period based on the design spectral acceleration is discussed. For this purpose, the prototype STRP-2/4 with aspect ratios 12 and 3.0 in the length and width direction is considered. The relationship between the horizontal stiffness and the isolator height is obtained from the results of numerical analysis of STRP-2/4 as shown in Tables 5 and 6 and the similitude law with different scale factors. A rigid mass that produces 5.0 MPa axial compression is considered in all bearing heights.

The isolator heights and respective isolation periods are checked for a target level of spectral acceleration by the iterative method such that the nominal shear strain of the isolators remains within the allowable limits. The damping coefficients B_D, B_M in the longitudinal direction are taken as 1.29 and 1.20, corresponding to 12% and 9% effective damping ratios, respectively. The respective values in the transverse direction are taken as 1.26 and 1.16 for 13% and 10% effective damping ratios. These values of damping correspond to 100% and 250% shear strain at which STRP-2/4 exhibits the minimum and maximum lateral stiffnesses within the DBE and MCE displacement limits.

Figure 18 shows the relationship between spectral acceleration, isolator height, isolation period, and maximum bearing displacement. The horizontal axis of these plots is the required isolator height for the DBE level spectral acceleration, as shown in Fig. 18(a). It indicates that the required isolator height increases with an increase of spectral acceleration. An increase in elastomer height causes lengthening the isolation period as shown in Fig. 18(b). It shows that a 72 mm thick isolator (864 mm ×216 mm) at 0.4 g DBE level acceleration offers isolation periods of 1.10 s and 1.25 s in the longitudinal and transverse directions, respectively. At the MCE level, the respective period for the same isolator is also longer than 1.0 s. Therefore, 72 mm can be regarded as the minimum height of the STRP isolator to meet the effectiveness seismic isolation at DBE level acceleration up to 0.4 g. At 0.65 g DBE acceleration, the minimum height is 180 mm, which provides isolation periods around 1.5 s and 2.0 s in the longitudinal and transverse direction, respectively. Figure 18(c) shows the maximum bearing displacement for DBE and MCE level spectral accelerations up to 0.65 g and 0.975 g, respectively. The maximum shear strain of the isolator is confirmed to be well within the allowable limits of 150% (DBE) and 250% (MCE). In particular, the maximum shear strain is substantially lower than 250%, implying that the isolator shows no slippage or instability under 5.0 MPa compression, even in the case of MCE. Therefore, the assumed strip-shaped STRP isolators subjected to 5.0 MPa compression can satisfactorily be used at a DBE level spectral acceleration up to 0.65 g by utilizing an appropriate height up to 180 mm.

A similar set of plots for a square-shaped isolator (Group-II in Table 1) with different heights is shown in Fig. 19. An aspect ratio of 3.0 and a vertical load that produces 5.0 MPa pressure are considered for all heights. From Table 7, minimum values of effective damping ratios of 13% and 10% corresponding to the minimum and maximum stiffnesses are assumed for each isolator. Figure 19(b) indicates that for an isolator of six STRP stacks (216 mm ×216 mm), a height of 72 mm is required for 0.35 g DBE level spectral acceleration that offers periods of 1.36 s and 1.14 s at DBE and MCE levels, respectively. At 0.56 g DBE acceleration, the required height is 192 mm that provides an isolation period around 2.14 s. The maximum shear strain for all height and respective acceleration shown in Fig. 19(c) remains within the allowable limits for DBE and MCE levels.

The plots are helpful in the preliminary design of a strip-shaped STRP isolator with aspect ratios of 12 and 3.0 in the length and width directions, respectively, or a square-shaped bearing with aspect ratio 3.0, for a vertical load equivalent to 5.0 MPa. The total plan area of the isolator can be distributed based on column force

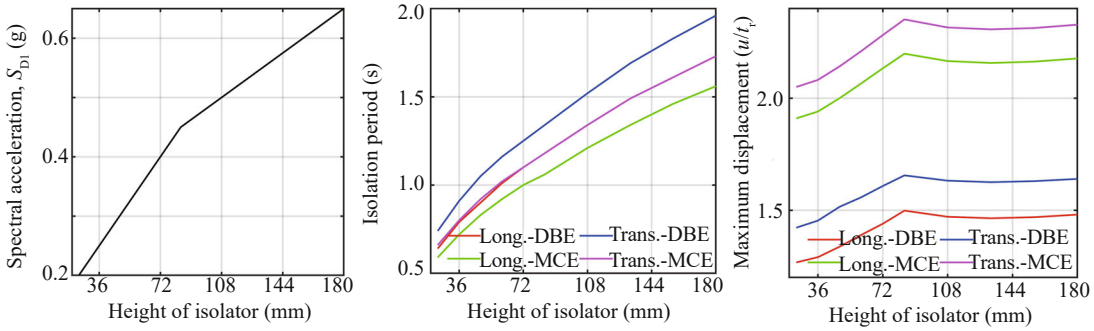

(a) Height vs spectral acceleration (b) Height vs isolation period (c) Height vs Max. isolator displacement

Fig. 18 Relation between spectral acceleration, height, period and displacement demand in strip-shaped isolator

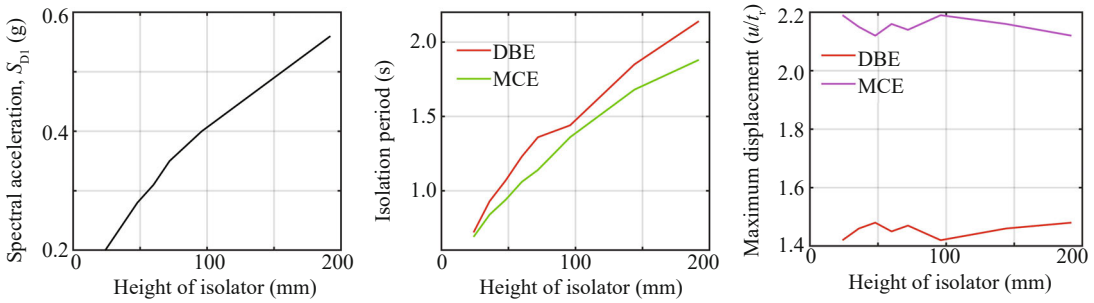

(a) Height vs spectral acceleration (b) Height vs isolation period (c) Height vs Max. isolator displacement

Fig. 19 Relation between spectral acceleration, height, period and displacement demand in square-shaped isolator

such that pressure on the individual bearing becomes nearly 5.0 MPa, and an aspect ratio exceeding 3.0. This change in the aspect ratio does not affect the period or maximum nominal shear more than 10%–15%, as seen in the previous section. However, if the average pressure within the isolators maintains 5.0 MPa, then the global isolation period remains unchanged. Note that a higher aspect ratio is preferable because it enhances the stability and safety margin. The orientation of the bearing and the direction of loading can also affect these results.

9 Conclusions

A series of 3-D FE analyses of STRP isolator models with various length-to-width ratios are conducted to investigate the influences of the STRP isolator shape on the performance against cyclic lateral loads. A friction-based model of isolators is developed using a contact model to represent the unbonded condition. The FE model is validated by comparing the analytical and experimental results, showing sufficient accuracy for the unbonded STRP isolator′s preliminary design. The isolators are analyzed under the conditions of 250% lateral shear and 5.0 MPa static compression. The findings from the FE analysis can be summarized as follows:

■ The modified stiffness solution represents the horizontal stiffness of square-shaped STRP isolators. The progressive rollover deformation of STRP isolators for displacement exceeding 150% shear increases the lateral stiffness.

■ The minimum stiffness of the strip-shaped STRP isolator in the transverse and longitudinal directions is in the range of 0.65–0.75 and 0.90–1.0 times of that calculated by the effective shear modulus, and the minimum equivalent damping ratio is about 10% within the shear strain range of 1.0–1.5. Stack numbers exceeding three have a negligible effect on the lateral stiffness of a square-shaped bearing with an aspect ratio of 3.

■ The dependence of stiffness on the length-to-width ratio is more significant in the longitudinal direction than the transverse direction. The stiffness in the longitudinal direction is 1.15–1.40 times that of stiffness in the transverse direction. When the length-to-width ratio increases from unity to 10, stiffness in the longitudinal direction increases by 37%–58% and decreases by 12% in the width direction.

■ At 250% shear level, an average reduction of the effective damping ratios is 38% and 33% in the longitudinal and transverse directions, respectively, whereas it is 52% in the square-shaped bearings. The dependence of damping on the length-to-width ratio exceeding 4.0 or stack numbers exceeding 3 is insignificant.

■ At site conditions of class C and D of the ASCE/SEI 7-10, the periods of base isolated structure are longer than 1.11s at DBE and MCE levels for 96 mm thick strip-shaped isolators. The maximum shear strain of the same isolators almost satisfies the allowable limit of 150% and 250% at DBE and MCE levels, respectively, at site class

C with S_1=0.40 and at site class D with S_1=0.40 and 0.50. The period and demand displacements in the transverse direction are about 12%–15% and 10%–15% larger than that of the longitudinal direction. The bearing′s displacement for a length-to-width ratio increases from unity to 10 and decreases by 10%–15%.

■ For a six-stack STRP isolator with aspect ratios of 12 and 3 in the length and width directions, respectively, 72 mm is the minimum height for a period longer than 1.0 s. The permissible DBE level acceleration is 0.4 g within the allowable displacement limits.

This research work is carried out through FE analysis based on experimental elastomer properties. For a comprehensive understanding of lateral performance and displacement demand of STRP base isolators, an experimental study should be carried out for different length-to-width ratios and different numbers of STRP stacks. The authors also suggest that it is important to determine the viscoelastic and Mullin damage parameters of STRP through laboratory experiments.

References

AASHTO-LRFD (2014), *LRFD Bridge Design Specifications, 7th Ed*., Washington, D. C., USA.

Al-Anany YM and Tait MJ (2015), "A Numerical Study on the Compressive and Rotational Behavior of Fiber Reinforced Elastomeric Isolators (FREI)," *Composite Structures*, **133**: 1249–1266.

Al-Anany YM, Van Engelen NC and Tait MJ (2017), "Vertical and Lateral Behavior of Unbonded Fiber-Reinforced Elastomeric Isolators," *Journal of Composite for Construction*, **21**(5): 1–11.

ASCE/SEI 7-10 (2010), *Minimum Design Loads for Buildings and Other Structures*, *ASCE*, 1801 Alexander Bell Drive, Reston, Virginia, USA.

Ashkezari GD, Aghakouchak AA and Kokabi M (2008), "Design, Manufacturing and Evaluation of the Performance of Steel Like Fiber Reinforced Elastomeric Seismic Isolators," *Journal of Material Processing Technology*, **197**: 140–150.

Baranowski P, Bogusz P, Gotowicki P and Malachowski J (2012), "Assessment of Mechanical Properties of Offroad Vehicle Tire: Coupons Testing and FE Model Development," *Acta Mechanica et Automatica*, **6**(2): 17–22.

Bandyopadhyay S, Sengupta A and Reddy GR (2015), "Performance of Sand and Shredded Rubber Tire Mixture as a Natural Base Isolator for Earthquake Protection," *Earthquake Engineering and Engineering Vibration*, **14**(4): 683–693.

CAN/CSA-S6-06 (2006), *Canadian Highway Bridge Design Code*, Canadian Standard Association, Ontario, Canada.

Calabrese A, Spizzuoco M, Serino G, Corte GD and Maddaloni G (2015), "Shaking Table Investigation of a Novel, Low-Cost, Base Isolation Technology Using Recycled Rubber," *Structural Control Health Monitoring*, **22**(1): 107–122.

De la Llera JC, Lüders C, Leigh P and Sady H (2004), "Analysis, Testing, and Implementation of Seismic Isolation of Buildings in Chile," *Earthquake Engineering and Structural Dynamics*, **33**(5): 543–574.

Das A, Dutta A and Deb SK (2014), "Performance of Fiber-Reinforced Elastomeric Base Isolators Under Cyclic Excitation," *Structural Control Health Monitoring*, **22**: 197–220.

Eurocode 8 (2004), *Design of Structures for Earthquake Resistance*, BS EN 1998-1: 2004.

Feng WW and Hallquist JO (2014), "Determining the Material Constants for Mullin Effect in Rubber Part One: Uniaxial," *13th International LS-DYANA Users Conference,* June 8-10, 2014, Dearborn, MI, USA.

Gerhaher U, Strauss A and Bergmeister K (2011), "Verbesserte Bemessungsrichtlinien für Bewehrte Elastomerlager. *Bautechnik*," **88**(7): 451–458. (in German)

Glenn Elert (1998–2006), "The Physics Hypertextbook," *http://hypertextbook.com/physics/mechanics/friction/*, Cited 01 Dec 2006.

Igarashi A, Matsushima H and Dang J (2013), "Influence of Loading Direction on the Seismic Performance of Rectangular STRP Isolators," *Journal of Applied Mechanics*, **16**(2): 425–434.

Karayel V, Yuksel E, Gokce T and Shahin F (2017), "Spring Tube Braces for Seismic Isolation of Buildings," *Earthquake Engineering and Engineering Vibration*, **16**(1): 219–231.

Kelly JM (1997), *Earthquake-Resistant Design with Rubber*, *2nd Ed*., Springer-Verlag, London, UK.

Kelly JM (1999), "Analysis of Fiber-Reinforced Elastomeric Isolators," *Journal of Seismology and Earthquake Engineering*, **2**(1): 19–34.

Kelly JM (2002), "Seismic Isolation Systems for Developing Countries," *EERI Distinguished Lecture*, *Earthquake Spectra*, **18**(3): 385–406.

Kelly JM (2003), "Tension Buckling Multilayer Elastomeric Bearings," *Journal of Engineering Mechanics*, **129**(12): 1363–1368.

Kelly JM and Takhirov SM (2001), "Analytical and Experimental Study of Fiber Reinforced Strip Isolators," *PEER Report 2002/11*, Dept. of Civil and Environmental Engineering, University of California, Berkeley, USA.

Kim B, Lee SB, Lee J, Cho S, Park H, Yeom S, and Park SH (2012), "A Comparison Among Neo-Hookean Model, Mooney Rivlin Model, and Ogden Model for Chloroprene Rubber," *International Journal of Precision Engineering and Manufacturing*, **13**(5): 759–764.

Kim NS, Lee J-H and Chang SP (2009), "Equivalent Multi-Phase Similitude Law for Pseudodynamic Test on Small Scale Reinforced Concrete Models," *Engineering*

Structures, **31**(4): 834–846.

Konstantinidis and Kelly JM (2014), "Advances in Low-Cost Seismic Isolation with Rubber," *10th U.S. National Conference on Earthquake Engineering Frontiers of Earthquake Engineering*, July 21–25, Anchorage, Alaska, USA.

May PJ (2002), "Barriers to Adoption and Implementation of PBEE Innovations," *PEER Rep. 2002/20*, Pacific Earthquake Engineering Research Center, University of California, Berkeley, USA.

Meschke G, Payer HJ and Mang HA (1997), "3D Simulations of Auto-mobile Tires: Material Modeling, Mesh Generation and Solution Strategies," *Tire Science and Technology*, TSTCA, **25**(3): 154–176.

Mishra HK (2012), "Experimental and Analytical Studies on Scrap Tire Rubber Pads for Application to Seismic Isolation of Structures" *PhD Thesis*, Kyoto University, Japan.

Mishra HK, Igarashi A, Matsushima H (2013a), "Finite Element Analysis and Experimental Verification of the Scrap Tire Rubber Pad Isolator," *Bulletin Earthquake Engineering*, **11**(2): 687–707.

Mishra HK and Igarashi A (2013b), "Lateral Deformation Capacity and Stability of Layer-Bonded Scrap Tire Rubber Pad Isolators Under Combined Compressive and Shear Loading," *Structural Engineering and Mechanics*, **48**(4): 479–500.

Mishra HK, Igarashi A, Ji D and Matsushima H (2014), "Pseudo-Dynamic Testing for Seismic Performance Assessment of Buildings with Seismic Isolation System Using Scrap Tire Rubber Pad Isolators," *Journal of Civil Engineering and Architecture*, **8**(1): 73–88.

MSC. Marc-Mentat (2018), "*Theory and User Information*," Vol. A, Santa Ana, CA: MSC Software Corporation.

Ngo TV, Dutta A and Deb SK (2017), "Evaluation of Horizontal Stiffness of Fibre-Reinforced Elastomeric Isolators," *Earthquake Engineering and Structural Dynamics*, **46**: 1747–1767.

Osgooei PM, Tait MJ, and Konstantinidis D (2014), "Finite Element Analysis of Unbonded Square Fiber-Reinforced Elastomeric Isolators (FREIs) Under Lateral Loading in Different Directions," *Composite Structure*, **113**: 164–173.

Pan P, Zamfirescu D, Nakashima N, Nakayasu N and Kashiwa H (2005), "Base–Isolation Design Practice in Japan: Introduction to the Post–Kobe Approach," *Journal of Earthquake Engineering*, **9**(1): 147–171.

Pauletta M, Cortesia A and Russo G (2015): Roll-Out Instability of Small Size Fiber-Reinforced Elastomeric Isolators in Unbonded Applications, *Engineering Structures*, **102**: 358–368.

Pistolas GA, Pitilakis K and Anastasiadis A (2020), "A Numerical Investigation on the Seismic Isolation Potential of Rubber/Soil Mixtures," *Earthquake Engineering and Engineering Vibration*, **19**(4): 683–704.

Russo G, Pauletta M and Cortesia A (2013), "A Study on Experimental Shear Behavior of Fiber-Reinforced Elastomeric Isolators with Various Fiber Layouts, Elastomers and Aging Conditions," *Engineering Structure*, **52**: 422–433.

Simo JC (1987), "On a Fully Three-Dimensional Finite Strain Viscoelastic Damage Model: Formulation and Computational Aspects," *Computer Methods in Applied Mechanics and Engineering*, **60**: 153–173.

Skinner RI, Robinson WH and McVerry GH (1993), *An Introduction to Seismic Isolation*, Wiley, Chichester, UK.

Spizzuoco M, Calabrese A and Serino G (2014), "Innovative Low-Cost Recycled Rubber-Fiber Reinforced Isolator: Experimental Tests and Finite Element Analyses," *Engineering Structure*, **76**(1): 99–111.

Strauss A, Apostolidi E, Zimmermann T, Gerhaher U and Dritsos S (2014), "Experimental Investigations of Fiber and Steel Reinforced Elastomeric Bearings: Shear Modulus and Damping Coefficient," *Engineering Structures*, **75**: 402–413.

Toopchi-Nezhad H (2014), "Horizontal Stiffness Solutions for Unbonded Fiber Reinforced Elastomeric Bearings," *Structural Engineering and Mechanics*, **49**(3): 395–410.

Toopchi-Nezhad H, Drysdale RG and Tait MJ (2009a), "Parametric Study on the Response of Stable Unbonded-Fiber Reinforced Elastomeric Isolators (SU-FREIs)," *Journal of Composite Materials*, **43**(15): 1569–1587.

Toopchi-Nezhad H, Tait MJ, Drysdale RG (2008a), "Lateral Response Evaluation of Fiber-Reinforced Neoprene Seismic Isolators Utilized in an Unbonded Application" *Journal of Structural Engineering*, *ASCE*, **134**(10): 1627–1637.

Toopchi-Nezhad H, Tait MJ and Drysdale RG (2008b), "Testing and Modeling of Square Fiber-Reinforced Elastomeric Seismic Isolators," *Structural Control Health Monitoring*, **15**(6): 876–900.

Toopchi-Nezhad H, Tait MJ and Drysdale RG (2009b), "Shake Table Study on an Ordinary Low-Rise Building Seismically Isolated with SU-FREIs (Stable Unbonded-Fiber Reinforced Elastomeric Isolators)," *Earthquake Engineering and Structural Dynamics*, **38**(11): 1335–1357.

Toopchi-Nezhad H, Tait MJ and Drysdale RG (2011), "Bonded Versus Unbonded Strip Fiber Reinforced Elastomeric Isolators Finite Element Analysis," *Composite Structures*, **93**(2): 850–859.

Tsai HC and Hsueh SJ (2001), "Mechanical Properties of Isolation Bearings Identified by a Viscoelastic Model," *International Journal of Solids and Structures*, **38**: 53–74.

Tsai HC and Kelly JM (2002), "Stiffness Analysis of Fiber-Reinforced Rectangular Seismic Isolators,"

Journal of Engineering Mechanics, *ASCE*, **128**(4): 462–470.

Tsang HH, Lo, SH, Xu X and Sheikh MN (2012), "Seismic Isolation for Low-to-Medium-Rise Buildings Using Granulated Rubber–Soil Mixtures: Numerical Study," *Earthquake Engineering Structural Dynamics*, **41**(14): 2009–2024.

Turer A and Özden B (2007), "Seismic Base Isolation Using Low-Cost Scrap Tire Pads (STP)," *Materials and Structures*, **41**(5): 891–908.

Van Engelen NC, Tait MJ and Konstantinidis D (2015), "Model of the Shear Behavior of Unbonded Fiber-Reinforced Elastomeric Isolators," *Journal of Structural Engineering*, *ASCE*, **141**(7): 1–11.

Walters Forensic Engineering (2006), "Skidmark Analysis and Braking," http://www.waltersforensic.com/articles/accident_reconstruction/vol1-no8.htm. Cited 01 Dec 2006

Xiao H, Butterworth JW and Larkin T (2004), "Low-Technology Techniques for Seismic Isolation," *New Zealand Society of Earthquake Engineering Conference*, Paper No. 36.